journal

J. Am. Ceram. Soc., **84** [5] 996–1003 (2001)

Electromechanical Properties of a Ceramic d_{31}-Gradient Flextensional Actuator

Xiaoping Li,[*,‡] James S. Vartuli,[‡] David L. Milius,[‡] Ilhan A. Aksay,[*,‡] Wan Y. Shih,[*,‡] and Wei-Heng Shih[*,†]

Department of Materials Engineering, Drexel University, Philadelphia, Pennsylvania 19104-2875 and Department of Chemical Engineering and Princeton Materials Institute, Princeton University, Princeton, New Jersey 08544-5263

We examined the static axial displacement of a ceramic d_{31}-gradient flextensional transducer both experimentally and theoretically. Two lead zirconate titanate systems, (PZT)/PZT and PZT/ZnO, were studied. The PZT/PZT transducers consisted of two PZT layers of different d_{31} coefficients. The PZT/ZnO transducers consisted of a PZT and a ZnO layer. The PZT/PZT transducers were of an inner-type dome structure. The PZT/ZnO transducers were either flat, or had an inner- or outer-type dome structure by varying the thickness ratio between the two layers or the Sb_2O_3 content in the ZnO layer. An inner (outer)-type transducer has the large-d_{31} layer on the inside (outside) of the dome structure. For the PZT/PZT transducers, the axial displacement varied with the thickness ratio and reached a maximum when the two layers had similar thickness, in agreement with the calculations. With a conductive nonpiezoelectric layer, the PZT/ZnO transducers had higher axial displacements, which varied with the thickness ratio and the Sb_2O_3 content, than the PZT/PZT transducers. With 6 wt% Sb_2O_3, the transducers were flat and the measured displacements at various thickness ratios were similar to the calculated values. With 4 wt% Sb_2O_3, the transducers were of an outer type. The measured axial displacements were about twice the calculated values, suggesting an enhanced d_{31} value because of the tensile bending stress in the PZT layer. The scaled axial displacements of the PZT/ZnO transducers with 4 wt% Sb_2O_3 were comparable to that of the Rainbow transducers. With 8 wt% Sb_2O_3, the displacements of transducers with thin PZT layers ($\leq$0.3 mm) were lower than the calculated values because of increased conductivity in the PZT layer.

I. Introduction

In ACTUATION applications, it is desirable to have transducers that can generate large displacements while withstanding a sizable load. While the direct extensional piezoelectric actuators made from soft lead ziconate titanate (PZT) can withstand very high stresses, they only generate strains on the order of 10^{-4} under large electric fields ($\sim 10^6$ V/m). Even with the relaxor-based single-crystal materials,[1–3] such as $Pb(Zn_{1/3}Nb_{2/3})O_3$·$PbTiO_3$ (PZN–PT) and $Pb(Mg_{1/3}Nb_{2/3})O_3$·$PbTiO_3$ (PMN–PT), the strain level is at best one to two percent at extremely high electric fields ($\sim 10^7$ V/m). In contrast, traditional flextensional actuators[4] can generate large axial displacements but cannot withstand large forces, limiting their applications as actuators. The recent development of a new class of flextensional transducers, such as the Moonie,[5,6] the Rainbow,[7] the Cerambow,[8] and the Thunder,[9] has generated new interest in piezoelectric transducers.[10–14] All these transducers can convert the lateral-strain gradient that results from a nonuniform d_{31} distribution in the thickness direction into a large axial displacement. Additionally, because of their dome shape, higher loading capability than that of a traditional bimorph or unimorph[7,15] can be expected.

Although these new structures have demonstrated good displacing and loading capabilities, they are difficult to miniaturize. Furthermore, it is difficult to modify the d_{31} distribution of these transducers to further enhance their actuation performance. Aiming for ease of miniaturization and better control of the axial d_{31} distribution, we have developed a new ceramic d_{31}-gradient flextensional transducer.[16] The ceramic d_{31}-gradient transducer is composed of ceramic layers of different d_{31} coefficients that are copressed and cosintered. For example, a PZT/PZT d_{31}-gradient transducer is made of PZT layers of different d_{31} coefficients and a PZT/ZnO d_{31}-gradient transducer consists of PZT and ZnO layers. The transducers can exhibit large axial displacements comparable to that of the Rainbow actuators. Furthermore, by controlling the sintering kinetics of the copressed layers, a transducer can be made flat, domed with the higher-d_{31} layer on the inside (inner type) or on the outside (outer type) of the dome structure. The copressing and cosintering approach gives the ceramic d_{31}-gradient transducers several advantageous characteristics including strong and interlocking interlayer bonding, easy control of the d_{31} distribution in the thickness direction, easy miniaturization, and compatibility with the micro-electronic technology. The processing details and the microstructural characteristics of the ceramic d_{31}-gradient transducers are to be reported in a separate publication. The present article focuses on the characterization of the electric-field-induced displacement of the ceramic d_{31}-gradient transducers. An analytical model based on a previous study of the PZT/brass unimorph systems[17,18] was modified to analyze the experimental results.

II. Experimental Procedures

Two types of ceramic d_{31}-gradient transducers have been examined, namely, the E70/E63 and the E76/ZnO transducers. E63, E70 and E76 were EC-63, EC-70 and EC-76 PZT powders, respectively, (EDO Corporation, Salt Lake City, UT). The E70/E63 transducers consisted of two PZT layers of different d_{31} coefficients, i.e., the EC-70 PZT and the EC-63 PZT. The E76/ZnO transducers were laminates of PZT (EC-76) and ZnO (Aldrich, Milwaukee, WI) layers with Sb_2O_3 (Aldrich) as the sintering retardant for ZnO. By varying the Sb_2O_3 content in the ZnO or the thickness ratio between the PZT layer and the ZnO layer, the transducers could be made flat or domed with the PZT on the inside (inner type) or the outside (outer type) of the dome.

W. A. Schulze—contributing editor

Manuscript No. 189 533. Received February 22, 1999; approved December 15, 2000.

Supported by the Army Research Office Multidisciplinary University Research Initiative (ARO/MURI), under Grant No. DAAH04-95-1-0102.

[*]Member, American Ceramic Society.

[†]Dept. of Materials Engineering, Drexel University.

[‡]Dept. of Chemical Engineering and Princeton Materials Institute, Princeton University.

Monolithic PZT and ZnO samples were also characterized to provide basic material properties.

Electrodes were made by applying a thin silver paste (Heraeus, Inc., West Conshohocken, PA) on the two major faces of the transducers followed by heat treatment at 600°C for 20 min with a heating and cooling rate of 2°C/min. The edges of the samples were sanded to ensure that the top and bottom electrodes were well separated. Thin metal wires were soldered to the electrodes for measurements. All d_{31}-gradient transducers and monolithic PZT samples were poled with a field of 1.5×10^6–2×10^6 V/m at 110°C for 30 min. All measurements were conducted after the samples had aged at room temperature for more than 2 d after poling.

The piezoelectric coefficient, d_{31}, and the elastic compliance, s_{11}, of the monolithic PZT samples were deduced from the radial-mode resonance impedance spectra obtained with an impedance analyzer (HP4192A, Hewlett Packard, Santa Clara, CA). The dielectric constant was measured using an LCR meter (HP4275A multi-frequency inductance–capacitance–resistance (LCR) meter at 1 kHz, Hewlett Packard). The d_{33} coefficients of the monolithic PZT disks were obtained using a Pennebaker Model 8000 d_{33} Tester (American Piezo Ceramics, Inc., Mackeyville, PA). The conductivity of monolithic ZnO thin sheets and the d_{31}-gradient transducers was examined by measuring the dc *I–V* curves (Keithley 240A High Voltage Supply and a Keithley 196-system—digital multimeter (DMM) ammeter, Keithley Instruments Inc., Cleveland, OH) were used. The range of the applied voltage was 0–1.2 kV. The resolution of the ammeter was 1 nA. The axial displacement was generated by applying an electric field across the thickness of the actuator in the direction of the polarization and measured with a linear variable displacement transducer (LVDT, Model L500, Omega Engineering, Inc., Stamford, CT) with a resolution of about 1 μm. In the measurement, the tip of the LVDT was placed against the top of the dome with the concave side of the sample facing the supporting surface, and unipolar square-waveform electric fields were applied to the sample at 0.05 Hz. Displacements were recorded after three periods.

III. Results

(1) Monolithic Layers

Figure 1 shows the radial-mode impedance resonance spectra of three monolithic PZT circular disks where the impedance, $|Z|$, and the phase angle are plotted versus frequency. The f_r and f_a are the resonant and antiresonant frequencies, respectively, at which the phase angle goes to zero. The electromechanical coupling coefficient K_{31} is related to the quantity $(f_a - f_r)/f_r$. That E70 and E76 had a larger $f_a - f_r$ than E63 indicates that E70 and E76 has higher electromechanical coupling coefficients than E63. The d_{31} and s_{11}, are deduced from the resonance spectra using the IEEE standard method.[19] The d_{31} is calculated using $d_{31}^2 = K_{31}^2(\varepsilon_{33}\varepsilon_0 s_{11})^{1/2}$ where ε_0 is the permeability of free space, ε_{33} the dielectric constant in the thickness direction, and K_{31} the electromechanical coupling coefficient that is a function of the quantity $(f_a - f_r)/f_r$ which are deduced from the resonance spectra.[20] The elastic compliance, s_{11}, is related to f_s by $1/s_{11} = [\pi^2 L f_s(1 - \nu^2)\rho]/\eta_1^2$ where f_s is the frequency at which the reactant becomes zero; L, ρ, and ν are the diameter or length, density, and Poisson ratio of the disc, respectively, and $\eta_1 \cong 2$ is a root of an equation involving the Bessel functions and the Poisson ratio.[20] Because f_s is close to f_r, we approximate f_r as f_s. The deduced d_{31} and Young's moduli, Y_{11}, are listed in Table I. Dielectric measurements show that the E63 has a lower dielectric constant than the E70. The E63 also has a smaller d_{31} and d_{33} value than the E70. Therefore, it is possible to form a d_{31}-gradient transducer when layers of different piezoelectric coefficients are bonded together.

Figure 2 shows typical current-density-versus-electric field characteristics of monolithic PZT and ZnO samples under dc conditions. At electric fields $<4 \times 10^5$ V/m, the ammeter could not detect the current density of the 25.4 mm diameter and 1 mm thick PZT disks. Only when the electric field was $>5 \times 10^5$ V/m, the current density became detectable. For electric fields ranging 8×10^5–10×10^5 V/m, the conductivities of all PZT samples were on the order of 10^{-10} S/m, indicating that the PZT samples were electrical insulators. In contrast, the monolithic ZnO exhibited the typical varistor behavior. When the applied electric field was small, the current density was negligible. When the applied electric field exceeded 6×10^4 V/m, the current density increased sharply. A prebreakdown field was defined as the electric field above which the current density increased sharply. The ZnO sample shown in Fig. 2 had a prebreakdown field of $\sim 6 \times 10^4$ V/m. The prebreakdown fields of the ZnO samples varied with the Sb_2O_3 content. For the Sb_2O_3 contents studied, 4–8 wt%, the prebreakdown field ranged from 2.5×10^4–6×10^4 V/m. When the electric field exceeded the prebreakdown field, the conductivity of the ZnO quickly reached the order of 0.01 S/m, $\sim 10^8$ times higher than that of the PZT samples. Thus, at electric fields $>1 \times 10^5$ V/m, the ZnO layer can be treated as an electrical conductor relative to the PZT layers.

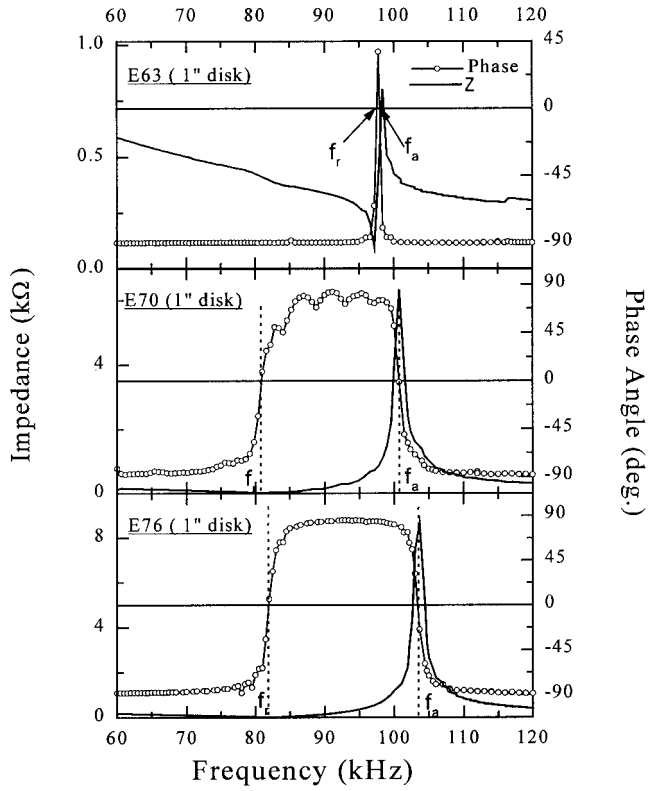

Fig. 1. Radial-mode resonance impedance spectra with both the impedance *Z* and the phase angle of E63, E70, and E76 monolithic PZT where f_a and f_r are the anti-resonant and resonant frequency, respectively.

Table I. Properties† of Various PZT Used in d_{31}-Gradient Transducers

Sample	ε_{33} (at 1 kHz)	Y_{11} (GPa)	d_{31} (pC/N)	d_{33} (pC/N)	σ_{dc} (10^{-10} S/m)
E63	1100	100	-30 ± 10	70	1.7 ± 0.2
E70	2800	63	-230 ± 30	540	1.9 ± 0.2
E76	3400	63	-250 ± 30	600	1.9 ± 0.2

†ε_{33} is the dielectric constant parallel to the polarization direction measured at 1 kHz, Y_{11} is the Young's modulus perpendicular to the polarization direction. d_{31} and Y_{11} are obtained using the radial-mode resonance spectra as described in the text, d_{33} is obtained with a d_{33} meter at 60 Hz, and σ is the dc conductivity measured at 25°C.

(2) Dome Configurations of d_{31}*-Gradient Actuators*

Because of the difference in the sintering kinetics between the two layers, the as-sintered d_{31}-gradient actuators could be flat or domed.[16] The dome-shape actuators could be classified as either

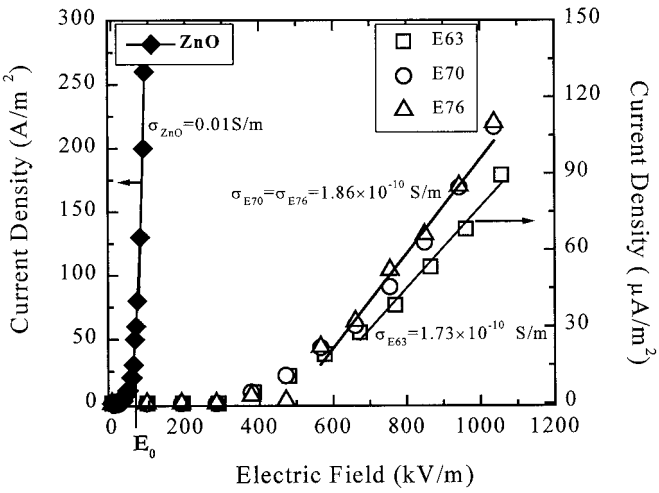

Fig. 2. Current density versus electric field for monolithic ZnO and PZT (E63, E70, and E76). The ZnO sample contained 8 wt% Sb_2O_3. E_0 indicates the prebreakdown field of the ZnO sample.

inner type or outer type. The inner (outer) type referred to the actuators that had the layer with a higher piezoelectric coefficient on the inside (outside) of the dome. A schematic of the inner-type and outer-type actuators is shown in Fig. 3. Because the d_{31} piezoelectric coefficient of the PZT was negative, an inner-type actuator moved up when the field was applied in the direction of the polarization while an outer-type actuator moved down. The type of dome structure, the radius of the dome curvature, *a*, along with the thickness ratio, α, between the two layers of the d_{31}-gradient actuators investigated are listed in Table II. The thickness ratio α was defined as the thickness of the layer with a smaller piezoelectric coefficient divided by that of the higher piezoelectric coefficient. For the E70/E63 systems, $\alpha = t_{E63}/t_{E70}$ and for the E76/ZnO systems, $\alpha = t_{ZnO}/t_{E76}$.

The α played an important role in the dome curvature of the E76/ZnO actuators. With a fixed Sb_2O_3 content in the ZnO layer, a large $\alpha = t_{ZnO}/t_{PZT}$ favored the outer type. With 4 wt% Sb_2O_3 in the ZnO layer, the actuators were outer type with the dome height increasing with an increasing $\alpha = t_{ZnO}/t_{PZT}$. When α became larger than unity, the actuators could not withstand the large sintering stress and cracked during sintering. With 6 wt% Sb_2O_3 in ZnO, the E76/ZnO actuators changed from the inner type to flat at small α and to outer type as α was increased.

The dome configurations were generally associated with a residual bending stress in the transducers. Assuming the bending deformation to be purely elastic, the bending strain of the samples could be estimated using $\varepsilon_b = t/2a$, where *t* was the total thickness of the transducer. The stress on the PZT surface was calculated using $\sigma_b = Y_{PZT}\varepsilon_b$, where Y_{PZT} was the Young's modulus of the

Table II. Dome Configurations of E70/E63 and E76/ZnO d_{31}-Gradient Actuators and Estimated Residual Bending Strain and Stress on the PZT Surface†

α	Configuration	*a* (cm)	ε (%)	Stress (MPa)
		PZT-E70/E63		
0.13	Inner	12	0.40	250
0.25	Inner	15	0.32	200
1.0	Inner	22	0.16	100
5.0	Inner	31	0.15	100
		PZT/ZnO (4 wt% Sb_2O_3)		
0.46	Outer	21	0.24	150
0.50	Outer	22	0.22	140
0.63	Outer	21	0.28	170
0.72	Outer	24	0.24	150
0.80	Outer	21	0.27	160
		PZT/ZnO (6 wt% Sb_2O_3)		
0.47	Inner	36	0.16	100
0.55	Flat	71	0.08	50
0.96	Flat	71	0.08	50
1.5	Outer	29	0.25	160
		PZT/ZnO (8 wt% Sb_2O_3)		
0.31	Inner	28	0.19	120
1.9	Outer	36	0.23	140

†α is the thickness ratio of the two layers in the d_{31}-gradient transducer ($\alpha = t_{E63}/t_{E70}$ for E70/E63 and $\alpha = t_{ZnO}/t_{E76}$ for E76/ZnO) and *a* is the radius of curvature of the domed transducer. The strain ε represents the residual bending strain on the PZT surface obtained by t/a, where *t* is the total thickness of the transducer and *a* is the radius of curvature. The residual bending stress on the PZT surface was estimated by $Y_{11}*\varepsilon$, where Y_{11} is the Young's modulus of PZT.

PZT. The estimated bending strain and bending stress in the d_{31}-gradient actuators are listed in Table II. The strain and stress on the concave (convex) side of the domed samples were compressive (tensile). Therefore, in the inner-type E70/63 system, the E70 layer that had a larger d_{31} and was on the concave side, was under a transverse compressive stress, while the E63 layer was under a tensile stress. The stress on the surface of the PZT layer for the sample with a small α was estimated as high as 250 MPa. As the α of the E70/E63 transducers increased to >1, the stress on the PZT surface decreased to <100 MPa. In the PZT/ZnO system, the PZT layer was under a tensile stress in the samples with a 4 wt% Sb_2O_3 content. With a higher Sb_2O_3 content in the ZnO layer, the stress changed with α. For a small α, the stress in the PZT side was tensile, while with a large α, the stress became compressive in the PZT side. The samples with an α ranging 0.5–1, having a less curved configuration, corresponded to minimum residual stress in the samples. The plastic deformation has been known to occur in PZT at stress levels 70–140 MPa.[21] The estimated tensile stress was in or exceeded the stress range where plastic deformation occurs, which indicated that the bending deformation was not entirely elastic. The present estimated stress only indicated the

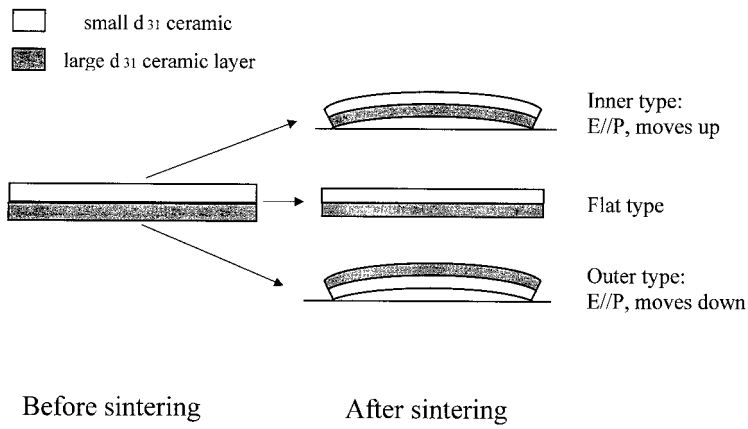

Fig. 3. Schematic of the dome configurations of the ceramic d_{31}-gradient transducers.

maximum of the possible bending stress. Nevertheless, the estimated bending stress gave an order of magnitude for the residual stress and allowed a more quantitative comparison of the stress effect among samples with different α's.

(3) Electric Field-Induced Axial Displacement of d_{31}-Gradient Transducers

Figures 4(a)–(c) illustrate the typical displacement performances of the d_{31}-gradient actuators under various driving-voltage conditions. The voltage increment was 100 V every 10 s. The loops shown in Figs. 4 (a)–(c) were recorded after the actuators had gone through several cycles and the loops had stabilized. Figure 4(a) shows the displacement versus voltage V under the unipolar condition between 0 and 800 V where the displacement was roughly linear in voltage but had considerable hysteresis. Under the bipolar driving condition between −400 and 400 V as shown in Fig. 4(b), the displacement-versus-voltage curve exhibited a symmetric hysteresis loop about the origin. However, at ±800 V as shown in Fig. 4(c), the actuator exhibited asymmetric displacement-voltage behavior. Similar asymmetric behavior has also been observed in poled $BaTiO_3$.[21] For the remainder of the results section, the displacement data were obtained in the unipolar condition, i.e., the electric field is applied in the same direction as the polarization direction with an operation frequency of 0.05 Hz.

The E70/E63 disk samples had the inner-type displacements, i.e., the dome moved up when the electric field was applied in the same direction as the polarization. The displacement of the PZT/PZT actuators versus $\alpha = t_{E63}/t_{E70}$ is shown in Fig. 5 as full circles. All E70/E63 disk actuators had a diameter of 25 ± 0.5 mm and a fixed total thickness $t = 1 \pm 0.02$ mm, and a dc voltage of 1000 V was applied across the thickness of the actuators. Clearly, the displacement of the PZT/PZT transducer had a strong thickness-ratio dependence and exhibited a maximum at $\alpha^* \approx 1$. A similar displacement maximum with respect to α has also been observed in PZT/metal unimorphs[18] and Rainbow transducers.[13] The α* at which the maximum axial displacement occurred depended on the elastic moduli and the conductivity of the constituent layers and, thus, can differ from system to system. More quantitative discussions are given in the modeling and discussion section.

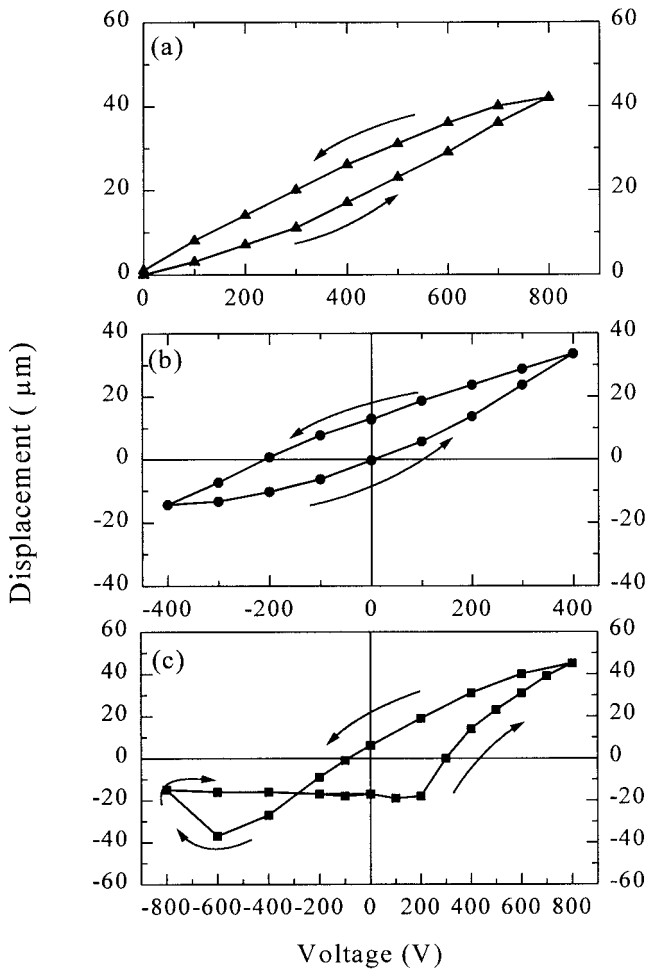

Fig. 4. Axial displacement of an E76/ZnO transducer with 4 wt% Sb_2O_3 in the voltage range (a) 0–800 V, (b) −400–400 V, and (c) −800–900 V.

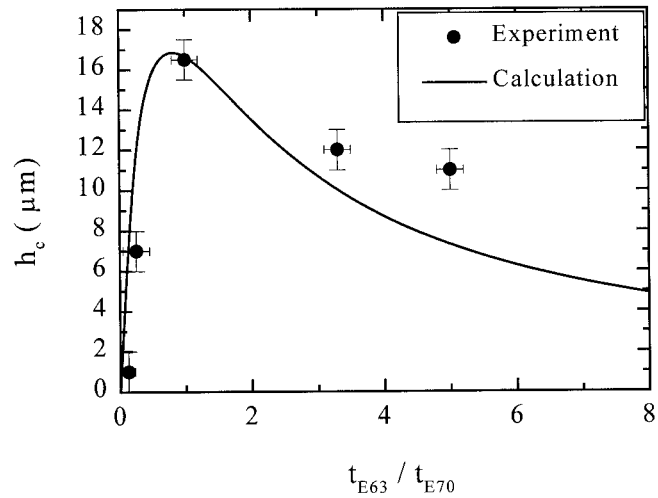

Fig. 5. Axial displacement, h_c, versus thickness ratio, $\alpha = t_{E63}/t_{E70}$, for the E70/E63 transducers at 1000 V. The samples had a total thickness, $t = 1 \pm 0.02$ mm and a diameter, $L = 25 \pm 0.5$ mm. Dotted line denotes the calculated values.

For engineering applications, a scaled displacement, *H*, was used to compare the performance of different actuators. The displacement was normalized by the factor, $V(L/t)^2$, where *V* was the applied voltage. H, stripped of the geometric factor and the applied voltage factor, allowed one to compare the effect of the gradient profile in the thickness direction as well as the materials properties more readily. The Rainbow transducers (Aura Systems, Inc., El Segundo, CA) have an $H = 1.42 \times 10^{-4}$ μm/V and were used as a reference. The highest *H* of the E70/E63 transducers at $\alpha^* \approx 1$ was 2.85×10^{-5} μm/V, ~20% that of the Rainbow transducers. Several factors were attributed to the smaller displacement of the E70/E63 transducers. Firstly, both layers in the E70/E63 transducers were piezoelectric. The difference in the piezoelectric coefficients between the two layers, $\Delta d_{31} = d_{31,E70} - d_{31,E63}$, was smaller than that in the Rainbow transducer which consisted of a high-d_{31} layer and a conductive nonpiezoelectric layer. Secondly, the low-d_{31} layer in the E70/E63 transducers was not conductive, which significantly lowered the effective electric field across the thickness of the higher-d_{31} layer. More quantitative discussions are given in the modeling and discussion section.

The E76/ZnO transducers consisted of an E76 PZT layer and a ZnO layer. Briefly, both the energy dispersion spectroscopy (EDS) and the scanning electron microscopy (SEM) analyses showed that the transducers had sharp interfaces about 50 μm wide between the PZT and the ZnO. The interfacial region was rich in antimony on the PZT side and poor in antimony on the ZnO side. A low concentration of Sb (<0.3 at.%) was present in the PZT layer. There was little evidence of interdiffusion of PZT and Zn beyond the interfacial region. The EDS analysis on the PZT layer showed oxygen depletion in the PZT layer in a zone ~200 μm wide near the interface. The presence of a reduction zone in the PZT layer near the interface was consistent with the high conductivity observed in the PZT/ZnO transducers with a thin PZT layer (≤0.3 mm) and a high antimony content (8 wt%) in the ZnO layer as we will show below. Details of the EDS and SEM analyses of the PZT/ZnO interface are to be reported in a separate publication. The varistor behavior exhibited by the ZnO layer is illustrated in Fig. 2. When the electric field exceeded 1×10^5 V/m in the ZnO

layer, the ZnO layer in the E76/ZnO transducer behaved like a conductive layer. Consequently, the E76/ZnO transducers could generate higher axial displacements than the E76/E63 transducers. For example, a E76/ZnO transducer with 4 wt% Sb_2O_3 generated a displacement as high as 40 μm at 600 V while a E70/E63 transducer exhibited a displacement of 16 μm at 1000 V.

Figure 6 shows the scaled displacements at the center, H_c versus $\alpha = t_{ZnO}/t_{PZT}$ of the E76/ZnO transducers with various Sb_2O_3 contents in the ZnO layer. All measurements were done at a fixed voltage of 600 V. All transducers had $t = 1 \pm 0.15$ mm and $L = 25.2 \pm 0.15$ mm. The transducers with 4 wt% Sb_2O_3 were outer type and exhibited the highest displacements. At $\alpha = 0.5$, the E76/ZnO actuator with 4 wt% of Sb_2O_3 exhibited $H_c = 11.2 \times 10^{-5}$ μm/V, ~80% that of the Rainbow transducer. However, with 4 wt% of Sb_2O_3 in ZnO, a thicker ZnO layer usually caused the transducer to crack after sintering. As a result, in Fig. 6, α was limited to the range 0.3–0.75 for samples with 4 wt% Sb_2O_3. Increasing the Sb_2O_3 amount in the ZnO layer to 5–6 wt% Sb_2O_3 reduced the sintering stress. Consequently, the axial displacements could be examined over a wider range of α. The H_c first increased with an increased α and then gradually leveled off when α reached ~1.5. The maximum H of the E76/ZnO transducers with 6 wt% of Sb_2O_3 was 8.4×10^{-5} μm/V, 25% lower than that obtained from samples with 4 wt% Sb_2O_3. Finally, when the Sb_2O_3 amount is further increased to 8 wt%, the H_c was reduced to the range 3.6×10^{-5}–6×10^{-5} μm/V, almost half the maximum H_c of E76/ZnO with 4 wt% of Sb_2O_3.

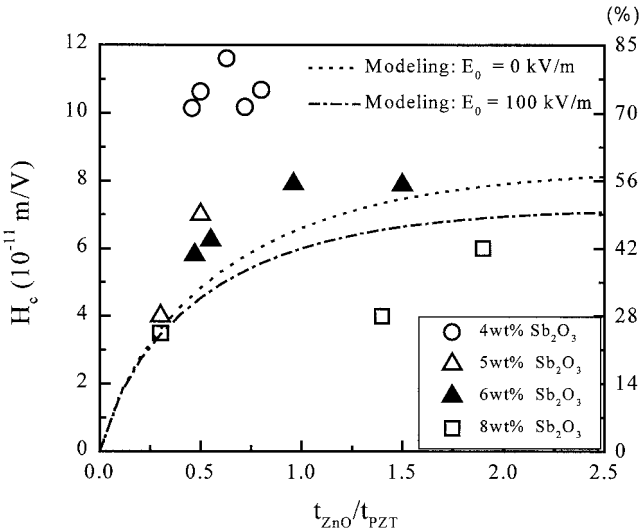

Fig. 6. Scaled axial displacement, H_c, versus $\alpha = t_{ZnO}/t_{E76}$, for the E76/ZnO transducers of various Sb_2O_3 doping. ((- - -) calculation result with no voltage drop in the ZnO layer and (— · — · —) calculated result with an electric field of 1×10^5 V/m in the ZnO layer). In the calculation, $Y_{ZnO} = 110$ GPa, $t = 1$ mm, $L = 25.4$ mm, and $V = 600$ V.

IV. Modeling and Discussion

Consider a transducer composed of two different layers as shown in Fig. 7. The top and bottom layers have thickness t_1 and t_2, and the Young's moduli Y_1 and Y_2, respectively. The electric field and the piezoelectric coefficient in the top and bottom layer are E_1 and E_2, and $d_{31,1}$ and $d_{31,2}$ respectively. Because of the different piezoelectric coefficients, a lateral strain difference, $d_{31,1}E_1 - d_{31,2}E_2$, develops between the two layers when a voltage V is applied across the thickness. This lateral-strain difference causes the transducer to bend, thus producing an axial displacement. Since most materials have a Poisson's ratio, ν, ~0.3, in the following discussion, we assume both layers to have the same Poisson's ratio. The axial displacement at the center of a disk, h_c, can be written as[17,18]

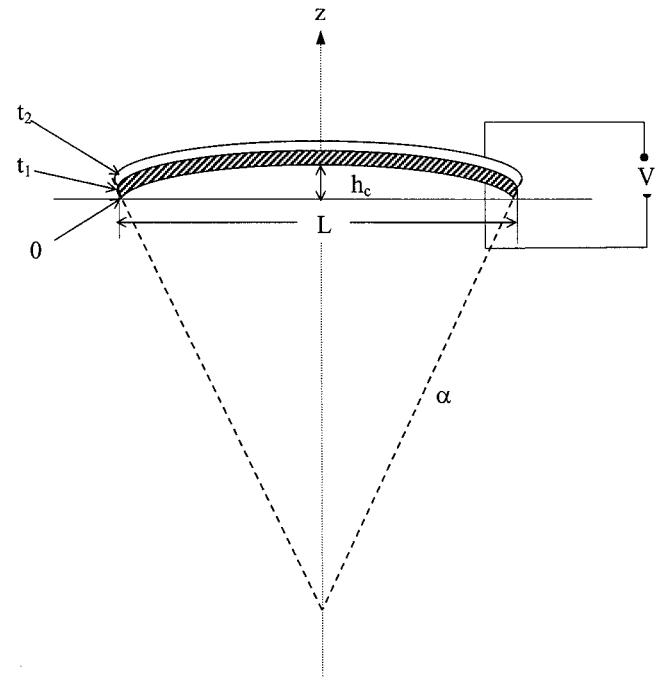

Fig. 7. Schematic of a d_{31}-gradient transducer.

$$h_c = \left(\frac{3L^2}{4}\right)\frac{Y_1Y_2t_1t_2(t_1+t_2)(d_{31,1}E_1 - d_{31,2}E_2)}{Y_1^2t_1^4 + Y_2^2t_2^4 + 2Y_1Y_2t_1t_2(2t_1^2 + 2t_2^2 + 3t_1t_2)}(1-\nu) \quad (1)$$

The conductivities of the top and bottom layers are σ_1 and σ_2, respectively. When a dc voltage V is applied across the thickness, the electric field in each layer is determined by the condition that the electric current is continuous, yielding

$$E_1 = \frac{\sigma_2}{\sigma_2 t_1 + \sigma_1 t_2}V = \frac{1}{t_1 + mt_2}V \quad (2)$$

and

$$E_2 = \frac{\sigma_1}{\sigma_2 t_1 + \sigma_1 t_2}V = \frac{m}{t_1 + mt_2}V \quad (3)$$

where $m = \sigma_1/\sigma_2$ is the conductivity ratio. In the present study, the total thickness, $t = t_1 + t_2$ is fixed. V is also fixed. If $k = Y_1/Y_2$, h_c at the disk center can be simplified as

$$h_c = \left(\frac{3}{4}\right)\frac{k\alpha(1+\alpha)^3(d_{31,1} - d_{31,2}m)}{[1 + k^2\alpha^4 + 2k\alpha(2 + 2\alpha^2 + 3\alpha)](1+\alpha m)}(1-\nu) \times\left(\frac{L}{t}\right)^2 V \quad (4)$$

h_c, can be divided into three factors. One of the factors is the geometry factor $(L/t)^2$, which depends on the aspect ratio α, of the transducer. The second factor is the external-driving-voltage factor, V. The third factor,

$$\frac{k\alpha(1+\alpha)^3(d_{31,1} - d_{31,2}m)}{[1 + k^2\alpha^4 + 2k\alpha(2 + 3\alpha + 2\alpha^2)](1+\alpha m)}(1-\nu)$$

relates to the gradient profile in the thickness direction as well as the properties of the individual layers, i.e., α, k, m, and the d_{31} piezoelectric coefficients of the layers. Given the $(L/t)^2$ and V, h_c can be further optimized through the third factor by varying the gradient profile in the thickness direction. To better see the effect of the gradient profile on the actuator's performance, the displacement at the center of the disk may be scaled with $(L/t)^2$ and V, as

$$H_c = \frac{h_c}{(L/t)^2 V} = \left(\frac{3}{4}\right) \frac{k\alpha(1+\alpha)^3(d_{31,1} - m d_{31,2})}{[1 + k^2\alpha^4 + 2k\alpha(2 + 3\alpha + 2\alpha^2)](1 + m\alpha)} \times (1 - \nu) \quad (5)$$

The H_c allows one to compare the effect of the gradient profile in the thickness direction more readily. In the following, the behavior of the E70/E63 transducers and the E76/ZnO transducers will be discussed separately.

(1) E70/E63 Transducers

Since the dc conductivity of the E70 PZT and that of the E63 PZT are similar, as shown in Fig. 2, we can approximate $m = 1$ for this system. The h_c becomes

$$h_{c,E70/E63} \cong \left(\frac{3}{4}\right) \frac{k\alpha(1+\alpha)^2 \Delta d_{31}}{1 + k^2\alpha^4 + 2k\alpha(2 + 3\alpha + 2\alpha^2)}(1 - \nu)\left(\frac{L}{t}\right)^2 V \quad (6)$$

where $\Delta d_{31} = d_{31,1} - d_{31,2}$ and

$$H_{c,E70/E63} \cong \left(\frac{3}{4}\right) \frac{k\alpha(1+\alpha)^2 \Delta d_{31}}{1 + k^2\alpha^4 + 2k\alpha(2 + 3\alpha + 2\alpha^2)}(1 - \nu) \quad (7)$$

From Table I, $\Delta d_{31} = 180$ pC/N, $k = Y_{E63}/Y_{E70} = 1.5$, $L = 25.4$ mm, $t = 1$ mm. Assuming $\nu = 0.3$, h_c versus $\alpha = t_{E63}/t_{E70}$, can be calculated from Eq. (6). The calculated h_c is plotted as a function of α in Fig. 5 as the solid line along with the experimental data (full circles). The calculated curve agrees with the experimental data quite well.

Meanwhile, the value of α where the maximum displacement occurs can be obtained by equating the derivative of h_c with respect to α with a fixed t to zero

$$\left(\frac{\partial h_c}{\partial \alpha}\right)_t = 0 \quad (8)$$

The solution of Eq. (8) gives the optimum thickness ratio, α^*:

$$\alpha^* = \left(\frac{1}{k}\right)^{1/2} \quad (9)$$

Using the value of $k = Y_{E63}/Y_{E70} = 1.5$ for the E70/E63, for this system $\alpha^* = 0.81$, which is very close to the experimental result.

While the general agreement between the calculation and the experimental results is good, the calculated curve is slightly higher than the experimental data points at small α and becomes progressively lower than the experiment data points at large α. Stress and electric fields can modify the d_{31} coefficients in the PZT layers. These effects are neglected in the calculations. The smaller than calculated h_c at small α may be attributed to the residual stress in the actuator associated with the dome structure and the higher than calculated h_c at large α may be attributed to the enhancement in the d_{31} coefficient by the applied electric field as discussed below. The piezoelectric properties of PZT ceramics with a composition near the morphotropic phase boundary (MPB) can vary significantly with the electric field and the stress. A unidirectional compressive stress has been shown to reduce the piezoelectric coefficients[22] and a transverse tensile stress is shown to enhance the domain reorientation and hence a larger d_{31}.[22] Li *et al.*[13] also suggested that the higher-than-expected h_c of the Rainbow transducer was a result of a stress-enhanced d_{31} in the actuator. Assuming that the bending of the actuator after sintering is purely elastic, the residual stress could be estimated from the dome curvature of the actuator. The residual stresses estimated from the dome curvatures are listed in Table II. The E70/E63 actuators had an inner-type structure. The convex side, the E63 layer with a small d_{31} coefficient, is under tension whereas the concave side, the E70 layer with a large d_{31} coefficient, is under compression. For samples with a small α, the compressive stress in the PZT layers are estimated as high as 250 MPa. Although the bending of the actuator may not be completely elastic, the estimated residual stress serves to indicate the order of magnitude of the stress level in the actuator that allows a quantitative comparison of the stress effect among samples with different thickness ratios. The high stress levels in the actuators with a small α can significantly affect the field-induced domain-switching behavior of the actuator. Presumably, the compressive stress in the E70 layer reduces while the tensile stress in the E63 layer enhances the domain switching capability. Consequently, the d_{31} gradient, Δd_{31}, of the E70/E63 transducers is reduced, resulting in a smaller-than-calculated h_c. As α increases, the actuator becomes less curved and thus has less stress effect. In such samples, the field effect become more significant. Generally, d_{31} increases with an increasing electric field. The d_{31} value obtained in the low-field impedance measurement is usually smaller than that obtained at the larger electric fields used in the displacement measurement. This field-dependent behavior is attributed to the non-180° domain motion,[23] which further relates to the stress in the PZT ceramics.[22] At the electric field of 1×10^6 V/m used in the experiment, field-enhanced domain switching could increase the d_{31}, resulting in h_c higher than the calculated values that are based on the low-field d_{31}.

(2) E76/ZnO Transducers

In the E76/ZnO system, the piezoelectric layer PZT is denoted as "1" and the nonpiezoelectric layer ZnO is denoted as "2". Since the conductivity of ZnO is much higher than the PZT, we assume the ZnO is conductive, i.e., $m = \sigma_{PZT}/\sigma_{ZnO} = 0$. This assumption is valid when the applied electric field is much larger than the prebreakdown field of the ZnO and when the ZnO layer thickness is smaller than the PZT layer. Under these conditions, H_c of E76/ZnO disk transducers becomes

$$H_{c,E76/ZnO} = \left(\frac{3}{4}\right) \frac{k\alpha(1+\alpha)^3 d_{31,1}}{1 + k^2\alpha^4 + 2k\alpha(2 + 3\alpha + 2\alpha^2)}(1 - \nu) \quad (10)$$

where $k = Y_{ZnO}/Y_{E76}$ and $\alpha = t_{ZnO}/t_{E76}$. In the calculation, we use $Y_{E76} = 62.5$ GPa and $Y_{ZnO} = 110$ GPa. The calculated H_c as a function of the α is plotted in Fig. 6 as the dotted line.

We also consider the case where the voltage drop in the ZnO layer is nonzero. In this case, a constant electric field E_0 is maintained in the ZnO layer, i.e., $E_2 = E_0$; $E_1 = V - E_0 t_2/t_1$. Substituting E_1 and E_2 into Eq. (1) and dividing the obtained h_c by $(L/t)^2 V$, we obtain

$$H_{c,E76/ZnO} = \frac{3}{4}\left(V - \frac{E_0 t\alpha}{1+\alpha}\right) \times \frac{k\alpha(1+\alpha)^3 d_{31,1}}{[1 + k^2\alpha^4 + 2k\alpha(2 + 3\alpha + 2\alpha^2)]V}(1 - \nu) \quad (11)$$

Using the parameters, $V = 600$ V, $E_0 = 1 \times 10^5$ V/m, H_c versus $\alpha = t_{ZnO}/t_{E76}$, is calculated and plotted as the dashed–dotted line in Fig. 6.

The two calculated curves are very close at small α. When the thickness of the ZnO increases, the voltage depletion in the ZnO layer increases resulting in a diminished electrical field in the PZT layer thus lowering the displacement. The 1×10^5 V/m prebreakdown field assumed in the calculation is overestimated. The experimental prebreakdown fields for the ZnO was 2×10^4–6×10^4 V/m (see Fig. 2) at various Sb_2O_3 contents. Even with such an overestimate, the two curves are still fairly close, indicating that ZnO can be effectively treated as a conductive layer.

Meanwhile, when comparing the experimental displacements with the calculated results for the E76/ZnO transducers, we find that the calculated values agree reasonably well with the experimental ones for samples containing 5–6 wt% Sb_2O_3 in the ZnO layer. For samples containing 4 wt% Sb_2O_3 in the ZnO layer, the experimental displacements are higher than predicted by the model while samples with 8 wt% Sb_2O_3 in the ZnO layer exhibit smaller displacements than the calculation predicts. We speculate that two factors may contribute to the discrepancy between the calculation and experiment for samples with 4 and 8 wt% Sb_2O_3 in the ZnO layer. One factor is the residual-bending-stress effect on the

domain switching. The other is the change in the conductivity of the PZT layer near the interface.

(A) Residual-Stress Effect: As we mention in a previous section, the sintering mismatch between the PZT and ZnO layers in the cosintered PZT/ZnO samples results in different dome configurations depending on the Sb_2O_3 content in the ZnO layer and α. The residual stress that results from the dome curvature could affect the non-180° domain reorientation capability of the PZT layer. A tensile stress enhances the electric-field-induced domain reorientation, whereas compressive stress suppresses it. The E76/ZnO transducers with 4 wt% Sb_2O_3 in the ZnO layer are the outer type where the PZT layer is on the outer side of the dome and is under tension. The tensile lateral stress tend to promote the non-180° domain reorientation and enhance the d_{31} effect in the PZT layer. As a result, the experimental displacement is higher than the calculated one since the d_{31} used in the calculations are for stress-free PZT. In contrast, with 8 wt% Sb_2O_3 in the ZnO layer, the samples become inner type. A compressive residual stress is present in the PZT layer, constraining the domain reorientation and, thus, reducing the d_{31} coefficient. The E76/ZnO samples with 5–6 wt% Sb_2O_3 in the ZnO layer have the smallest residual strain. These samples generally appear flat and the stress effect is minimal. Consequently, the calculated displacements, which did not take into account the stress effect, agreed quite well with the experiment.

(B) Conductivity Effect: The stress effect alone could not account for all the discrepancy between the experimental observation and the calculation. For example, the E76/ZnO sample with 8 wt% Sb_2O_3 in the ZnO layer is outer-type (implying a higher d_{31}) when $\alpha = t_{ZnO}/t_{E76}$ is larger than unity. However, the H_c of such samples were still smaller than those of the inner-type (implying a smaller d_{31}) E76/ZnO actuators with 6 wt% Sb_2O_3 in the ZnO layer. Such contradiction prompted us to examine another factor in the PZT/ZnO system, namely, the conductivity in the thickness direction. Figure 8 shows the current density versus voltage for two samples. Sample A is a E76/ZnO transducer with 4 wt% Sb_2O_3 in the ZnO layer and an E76-layer thickness of ~0.5 mm. Sample B is a E76/ZnO transducer with 8 wt% Sb_2O_3 in the ZnO layer and an E76-layer thickness of ~0.3 mm. Both samples have L = 25 mm and t = 1.1 mm. In Fig. 8, the electric field is calculated by dividing the voltage by the thickness of the PZT layer alone. The two samples have very different current-density-versus-voltage characteristics. Sample A with a smaller Sb_2O_3 content in the ZnO layer and a thicker PZT layer shows an insulator behavior $\leq 1.4 \times 10^6$ *V/m*, indicating the PZT layer is not conductive. The dc conductivity of the PZT layer in this sample is estimated to be $\sim 10^{-10}$ S/m. In contrast, for Sample B, the current density increases drastically with the applied electric field. This indicates that the Sb_2O_3 doping in the ZnO layer causes the PZT layer near the interface to become conductive. It is possible that the piezoelectric layer became conductive when the thickness of the Sb-affected layer is comparable to that of the PZT layer. This appears to be the case for sample B. Because of the increase in the conductivity, the electric field in the PZT layer is reduced, resulting in a decrease in the h_c.

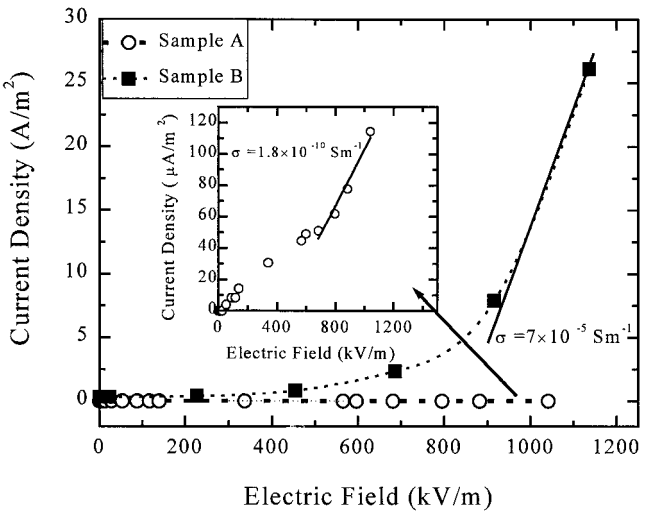

Fig. 8. Current density versus electric field for two E76/ZnO transducers. Sample A had 4 wt% Sb_2O_3 in the ZnO layer and Sample B had 8 wt% Sb_2O_3 in the ZnO. Electric field is obtained by dividing the applied voltage by the PZT thickness.

The discussions in the preceding sections indicate that the electric-field induced h_c of the PZT/ZnO actuators can be affected by both the residual stress and the change in the conductivity near the interfacial region. When $\alpha = t_{ZnO}/t_{E76}$ is small (i.e., thicker PZT layer) and the Sb_2O_3 doping amount in the ZnO layer is small, the residual stress effect dominates. As a result, the outer-type PZT/ZnO transducers with 4 wt% Sb_2O_3 in the ZnO layer exhibit higher h_c than the theoretical predictions. When $\alpha = t_{ZnO}/t_{E76}$ is large (i.e., thinner PZT layer) and the Sb_2O_3 doping is higher, the PZT layer become conductive. Consequently, the samples with 8 wt% Sb_2O_3 doping in the ZnO layer and $\alpha > 1$, exhibit lower h_c than the theoretical prediction.

V. Conclusions

We have examined both experimentally and theoretically the static axial displacements of flextensional ceramic d_{31}-gradient transducers of different gradient profiles. The PZT/PZT transducers consisted of two PZT layers of different piezoelectric coefficients with various thickness ratio α between the two layers. The PZT/ZnO transducers consisted of a highly piezoelectric PZT layer and a conductive ZnO layer with various α between the two layers and various Sb_2O_3 content in the ZnO layer. The PZT/PZT transducers were of an inner-type dome structure. The PZT/ZnO transducers were flat, or had an inner-type or outer-type dome structure, depending on α and the Sb_2O_3 content in the ZnO layer. For the PZT/PZT transducers, the h_c, which varies with α, exhibited a maximum when the two layers had similar thickness. The measured h_c of the PZT/PZT transducers were in good agreement with the model calculation. The combination of a highly piezoelectric layer with a conductive nonpiezoelectric layer gave the PZT/ZnO transducers higher h_c than the PZT/PZT transducers. For the PZT/ZnO transducers, the h_c not only varied with the layer α but also the Sb_2O_3 content in the ZnO layer. With 6 wt% Sb_2O_3 in the ZnO layer, the transducers were roughly flat. The measured h_c were in line with the calculated ones. With 4 wt% Sb_2O_3 doping in the ZnO layer, the transducers were of the outer-type dome structure. The measured h_c were about twice the calculated values. The enhanced h_c of the PZT/ZnO transducers with 4 wt% Sb_2O_3 were attributed to the outer-type dome structure where a tensile bending stress existed in the PZT layer. With $\alpha = t_{ZnO}/t_{E76} \approx 0.5$, the H_c of the PZT/ZnO transducers with 4 wt% Sb_2O_3 were comparable to that of the Rainbow transducers. With 8 wt% Sb_2O_3 in the ZnO layer, the measured h_c of samples with a thin PZT layer were lower than the calculated values. The lower-than-expected h_c in these transducers were attributed to the increased conductivity in the PZT layer near the PZT/ZnO interface when the ZnO layer had a higher than 6 wt% Sb_2O_3 content.

References

[1]V. A. Bokov and I. E. Myl'nikov, "Ferroelectric Properties of Monocrystals of New Perovskite Compounds," *Sov. Phys.-Solid State*, **2**, 2428–32 (1961).

[2]J. Kuwata, K. Uchino, and S. Nomura, "Phase Transitions in the $Pb(Zn_{1/3}Nb_{2/3})O_3$-$PbTiO_3$ Systems," *Ferroelectrics*, **37**, 579–82 (1981).

[3]Seung-Eek Park and Thomas R. Shrout, "Ultrahigh strain and Piezoelectric Behavior in Relaxor Based Ferroelectric Single Crystals," *J. Appl. Phys.*, **82** [4] 1804–11 (1997).

[4]J. M. Herbert, *Ferroelectric Transducers and Sensors*, Gordon and Breach Science, New York, 1982.

[5]Y. Sugawara, K. Onitsuka, S. Yoshikawa, Q. Xu, R. E. Newnham, and K. Uchino, "Metal-Ceramic Composite Actuators," *J. Am. Ceram. Soc.*, **75** [4] 996–98 (1992).

[6]A. Dogan, Q. Xu, K. Onitsuka, S. Yoshikawa, K. Uchino, and R. E. Newnham, "High Displacement Ceramic Metal Composite Actuators (Moonies)," *Ferroelectrics*, **156**, 1–6 (1994).

[7]G. H. Haertling, "Rainbow Ceramics: A New Type of Ultra-High Displacement Actuator," *Am. Ceram. Soc. Bull*., **73** [1] 93–96 (1994).

[8]B. W. Barron, G. Li, and G. H. Haertling, "Electromechanical Properties of PLZT-Based Cerambow Actuators"; presented at the Annual Meeting of American Ceramic Society, Cincinnati, OH, May 4–7, 1997 (Paper No. SXVII-015-97).

[9](a) R. F. Hellbaum, R. G. Bryant, and R. L. Fox, "Thin Layer Composite Unimorph Ferroelectric Driver and Sensor," U.S. Pat. No. 5 632 841, May 27, 1997. (b) R. G. Bryant, "Process for Preparing a Tough, Soluble, Aromatic, Thermoplastic Copolyimide," U.S. Pat. No. 5 639 850, June 17, 1997.

[10]K. Onitsuka, A. Dogan, Q. Xu, S. Yoshikawa, and R. E. Newnham, "Design Optimization for Metal-Ceramic Composite Actuator, 'Moonies'," *Ferroelectrics*, **156**, 37–42 (1994).

[11]C. Elissalde and L. E. Cross, "Dynamic Characteristics of Rainbow Ceramics," *J. Am. Ceram. Soc*., **78** [8] 2233–36 (1995).

[12]C. Elissalde, L. E. Cross, and C. Randall, "Structural-Property Relations in a Reduced and Internally Biased Oxide Wafer (Rainbow) Actuator Materials," *J. Am. Ceram. Soc*., **79** [8] 2041–48 (1996).

[13]G. Li, E. Furman, and G. H. Haertling, "Stress-Enhanced Displacement in the PLZT Rainbow Actuators," *J. Am. Ceram. Soc*., **80** [6] 1382–88 (1997).

[14]D. E. Dausch, "Ferroelectric Polarization Fatigue in PZT-Based Rainbows and Bulk Ceramics," *J. Am. Ceram. Soc*., **80** [9] 2355–60 (1997).

[15]P. L. Gould, *Analysis of Plates and Shells*; pp. 1–15. Prentice Hall, Upper Saddle River, NJ, 1999.

[16]J. S. Vartuli, D. L. Milius, X. Li, W.-H. Shih, W. Y. Shih, R. K. Prud'homme, and I. A. Aksay, "Processing of a High Displacement Ceramic-Ceramic Flextensional Actuator (PrinDrex)"; unpublished work.

[17]W. Y. Shih, W. H. Shih, and I. A. Aksay, "Scaling Analysis for the Axial Displacement and Pressure of Flextensional Transducers," *J. Am. Ceram. Soc*., **80** [5] 1073–78 (1997).

[18]X. Li, W. Y. Shih, I. A. Aksay, and W.-H. Shih, "Electromechanical Behaviors of PZT/Brass Plate Unimorph," *J. Am. Ceram. Soc*., **82** [7] 1733–40 (1999).

[19]"IEEE Standard on Piezoelectricity," ANSI/IEEE Standard 176-1987, Institute of Electrical and Electronic Engineers, New York, Jan. 29, 1988.

[20]A. J. Moulson and J. M. Herbert, *Electroceramics*; pp. 275–76. Chapman and Hall, London, 1990.

[21]B. Jaffe, W. R. Cook, Jr., and H. Jaffe, *Piezoelectric Ceramics*; p. 79, Fig. 5.15. Academic Press, London U.K. and New York, 1971.

[22]S. W. Meeks and R. W. Timme, "Effects of One-Dimensional Stress on Piezoelectric Ceramics," *J. Appl. Phys*., **46**, 4334 (1975).

[23]T. Tsurumi, Y. Kumano, N. Ohashi, T. Takenaka, and O. Fukunaga, "90° Domain Reorientation and Electric-Field-Induced Strain of Tetragonal Lead Zirconate Titanate Ceramics," *Jpn. J. Appl. Phys*., **36**, 5970 (1997). □